Design and Testing of a Propellant Feed System for the Lithium Lorentz Force Accelerator

Jeremy Mehl, 2015

Submitted to the
Department of Mechanical and Aerospace Engineering
Princeton University
in partial fulfillment of the requirements of
Undergraduate Independent Work.

Final Report

30 April 2015

Edgar Choueiri
Yiguang Ju
MAE 442
40 pages
Adviser Copy

This thesis represents my own work in accordance with University regulations.

Abstract

The Lithium Lorentz Force Accelerator (LiLFA) is a magnetoplasmadynamic thruster (MPDT) at Princeton University's Electric Propulsion and Plasma Dynamics Laboratory. The current piston-based lithium propellant feed system, though accurate, has proved to be buggy and unreliable. Therefore, a feed system using an electromagnetic pump has been designed to replace the piston-based pump. Operation of the pump has been tested using gallium as a surrogate metal, but the pump failed to achieve the required flow rate precision. A laser interferometer-based level measurement system was designed in parallel, but due to signal noise it was not useful as an instrument. Further work remains to determine whether an electromagnetic pump would be an effective replacement for the piston-based pump.

Acknowledgements

First, I would first like to thank my advisor, Professor Edgar Choueiri, for giving me the opportunity to conduct this research in his laboratory. Working in the EPPDyL was a highly enjoyable and enriching experience. I owe a great deal to the lab technician, Bob Sorenson, and to the graduate students for their advice and guidance. In particular, Will Coogan and Mike Hepler were incredibly helpful at every stage of the process. I am sincerely grateful for their mentorship. Additionally, I am picking up this project from summer student Nick Luzarraga; Nick provided helpful insights that became incorporated into this thesis.

This work would not have been possible without the support of the MAE department, the School of Engineering and Applied Science, and the Morgan W. McKinzie Senior Thesis Fund.

More broadly, I would like to express gratitude to my friends, who made my time at Princeton the best four years of my life. Finally, the ultimate credit goes to my family, for their constant care and support, as well as for encouraging and fostering my love for science.

Contents

List of Tables

List of Figures

List of Symbols

Chapter 1

Introduction

1.1 LiLFA Background

Electric spacecraft propulsion is a method of accelerating a spacecraft that uses energy, typically from solar arrays, to accelerate propellant to much higher exhaust velocities than chemical propulsion, thus allowing spacecraft to be much more fuel-efficient. That is, electric thrusters can give a spacecraft a much higher delta-v given the same amount of fuel.

The Lithium Lorentz Force Accelerator (LiLFA) is a magnetoplasmadynamic thruster (MPDT) at Princeton University's Electric Propulsion and Plasma Dynamics Laboratory. MPDTs are a class of electric thruster that use electric and magnetic fields to accelerate the propellant. MPDTs are an active topic of research because of their potential to offer both high thrust and high exhaust velocity.

MPDTs use a variety of different propellants, such as neon, argon, xenon, and lithium. The propellant feed system is a crucial component of the thruster because the propellant flow rate has a strong effect on the thrust produced. The LiLFA uses lithium propellant, which is circulated in liquid state and vaporized at the cathode of the thruster. Lithium is advantageous because of its low ionization potential. This means less energy is required to ionize the propellant—thus leaving more energy to accelerate the propellant. The disadvantage of lithium is that it is highly corrosive to many materials (and reacts readily with air or water), so special precautions must be taken in designing the propellant feed system.

(a) The propellant feed system.

(b) The thruster and solenoid.

Figure 1.1: Views inside the LiLFA tank.

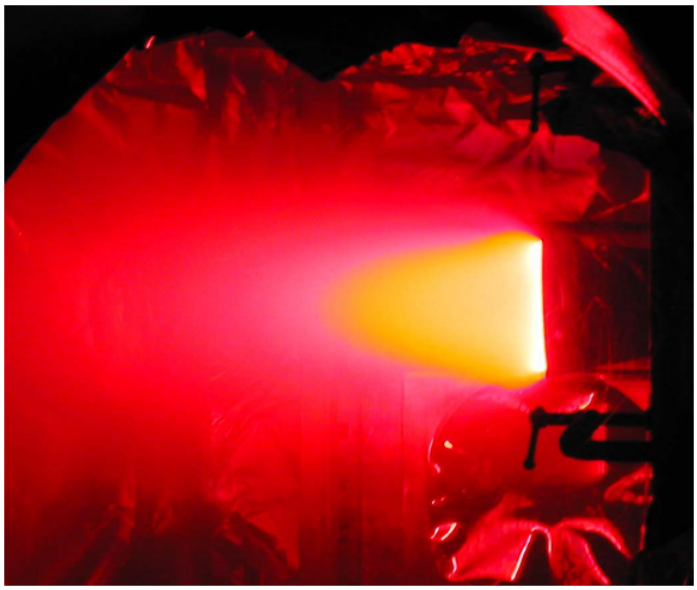

Figure 1.2: LiLFA firing.

1.2 Current LiLFA Feed System Setup

Figure 1.3 shows the current LiLFA feed system configuration. The liquid lithium propellant is circulated using a piston pump, where a piston sliding in a cylinder pushes lithium out of the cylinder and into the thruster. Lithium is loaded into a reservoir and passes through the reservoir line and a freeze valve (A) into the lithium chamber in the cylinder. Once the cylinder is loaded with lithium, freeze valve A is closed, and the piston, operated by the piston motor, pushes lithium down through the thruster line and into the cathode of the thruster.

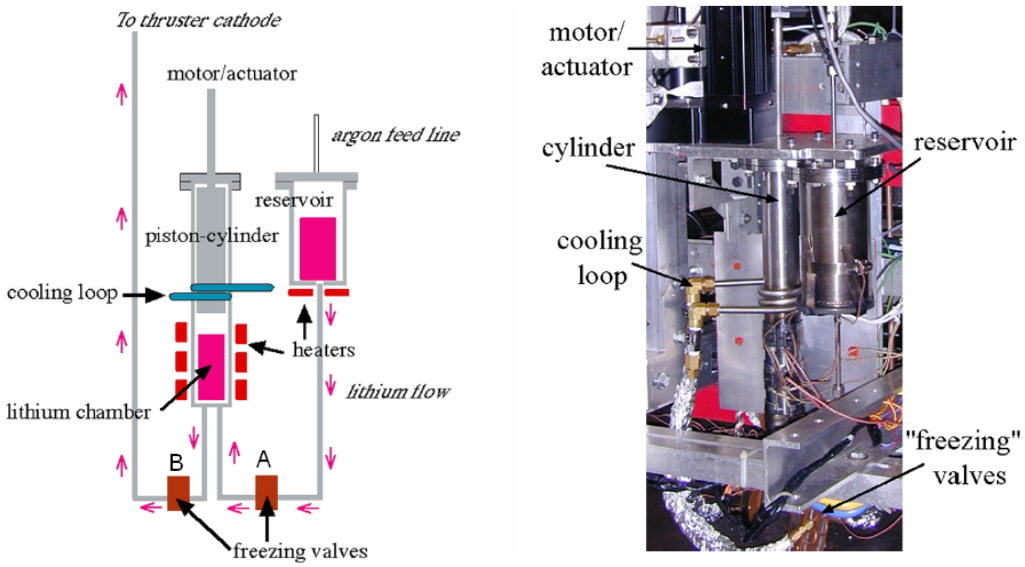

(a) Schematic

(b) Photo

Figure 1.3: LiLFA feed system. [4]

The piston pump is useful because the piston is operated by a stepper motor system capable of moving at velocities as slow as 1μm/s, thus giving very precise flow rate readings [4]. However, due to the corrosiveness of liquid lithium, a design compromise was made in the piston system, leading to a failure mode. In order to be compatible with lithium, the O-rings around the piston were chosen to be 304 stainless steel. However, 304 SS is too hard to seal properly in this case, so lithium will often leak around the sides of the piston. Once the lithium leaks, it can freeze, causing the piston to jam, in turn causing damage to the system.

Unfortunately, because of this, a large amount of effort is spent debugging the feed system instead of conducting experiments. This motivates the redesign of the feed system.

1.3 Goal of This Thesis

Therefore, it has been proposed as a design goal to, wherever possible, eliminate moving parts in contact with liquid lithium. An electromagnetic (EM) pump in conjunction with a laser interferometer-based mass flow meter was selected as the most promising candidate for a non-contact propellant feed system. This thesis will detail the design and testing process for an EM pump, with the goal of preparing it for integration into the LiLFA propellant feed system. Particular attention is paid to determine if the pump can achieve the desired flow rates of 10-100 mg/s with a precision of 0.5 mg/s.

Chapter 2 will investigate the theory and design considerations for a feed system utilizing an EM pump. Chapter 3 will summarize testing efforts for an EM pump with gallium. Chapter 4 will investigate the theory and design considerations for a laser interferometer-based level measurement instrument for liquid lithium. Chapter 5 will test this instrument with gallium. Chapter 6 will then summarize and give recommendations for future work.

For time management purposes, the pump and the flowmeter were developed in parallel.

Chapter 2

Theory and Design of EM Pump Feed System

2.1 Selection of Feed System Pressurization System

The pressurization system serves the straightforward purpose of forcing the propellant into the thruster in a controlled manner. It should be noted that, naturally, an electric thruster is intended to work in zero-g; but in the EPPDyL, gravity is a given constraint. Therefore, given the status of the LiLFA as a research instrument and not as a flight hardware project, techniques that use gravity are considered valid.

Early on, it was decided to avoid conventional mechanical pumps because they contain complex moving parts and seals which are incompatible with liquid lithium; therefore, these pumps are not better than the current piston pump. For the same reason, valves, which contain moving parts and seals, are discouraged.

There were several different candidate liquid pumping techniques that could replace the piston pump.

- **Passive control.** Liquid propellants can be circulated using surface tension and capillary forces, as described by Forrester and Barcatta [8]. The incorporation of such a system would require extensive modification of the LiLFA setup. Instead, a drop-in replacement for the original pump is preferred. Therefore passive control is outside the scope of this thesis.

- **Elastic diaphragm**. Two chambers are separated by an elastic diaphragm, with the propellant in one compartment and a pressurized gas in the other[4]. The pressure exerted on the propellant is controlled by modulating the pressure in the adjoining comparment, thus changing the shape of the diaphragm. No appropriate elastic material compatible with liquid lithium could be found, so this approach was abandoned.

- **Elevation**. In this approach, the reservoir is elevated above the thruster so that gravity serves as the pressurization system; control of the flow rate would then be achieved by a valve. However, as noted previously, valves are undesirable because they contain moving parts.

- **Electromagnetic (EM) pump**. Liquid metals are conductive, so they can carry current. They are also fluids, so a jxB (or Lorentz) body force applied to the fluid will cause it to accelerate or increase the pressure [4]. The chief advantage of the EM pump is that it has no moving parts in contact with lithium.

Given the problems with all other approaches, and the lack of obvious problems with the EM pump, it made sense to attempt to replace the piston pump with an EM pump.

(a) Assembled. Note iron yoke surrounding the assembly, providing structural support and intensifing the magnetic field.

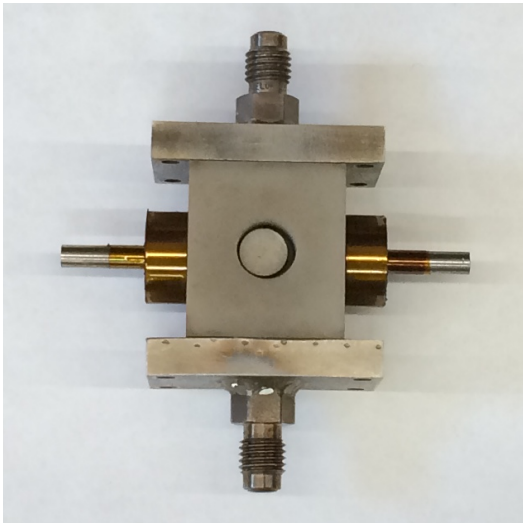

(b) Disassembled. Note electrodes on the east and west faces, pipe fittings on the north and south faces, and permanent magnets on the front and rear faces.

Figure 2.1: EM pump.

A prototype EM pump was lent to the EPPDyL for testing (see Figure 2.1). Markusic et al. [6] details the design of the pump and its initial testing. The pump is of the "DC conduction" type, the simplest type of EM pump. In the DC conduction pump, two electrodes in contact with the liquid metal introduce a current (j) into the fluid channel. Two magnets on opposing sides of the channel introduce a magnetic field (B) into the fluid channel. The interaction thus generates a jxB body force (note that j and B are perpendicular) in the fluid, accelerating it through the channel.

2.2 Feed System Design Criteria

The LiLFA is expected to operate at mass flow rates of $\mathcal{O}(10-100)$ mg/s. Therefore, this was set as a design point for the feed system: it must be able to achieve flow rates as low as 10 mg/s and as high as 100 mg/s. However, specifying a range is not very useful in the absence of a *precision*. Naturally, in order to reliably produce thrust, the feed system is expected to reliably achieve desired flow rates. Upcoming experiments require mass flow rates within ± 0.5 mg/s. Therefore, ± 0.5 mg/s was set as a design point for the feed system.

Therefore, the feed system will be designed to achieve flow rates in the range **10-100 mg/s**, with a precision of **±0.5 mg/s**.

lead into choice of apparatus, money constraints ripple, noise, etc does this even matter power supply maybe 16 bit has even more influence just say the daq we had only has 16 bits

2.3 Calculations for DC Power Supply

Current will be provided to the EM pump by a DC power supply. Since the mass flow is controlled by the modulation of current, the range requirement (10-100 mg/s) will determine the range of currents needed by the power supply, and the precision requirement (±0.5 mg/s) will determine the precision needed by the power supply. It will become clear below that the determination of specifications for the power supply is nontrivial.

2.3.1 Power Supply Range Requirement

In this section the required range of the DC power supply will be calculated.

The pressure P required to pump the lithium is the sum of the following components. This follows from Bernoulli's equation and the Darcy-Weisbach equation.

- Hydrostatic elevation pressure ρgh
- Dynamic pressure $\frac{1}{2}\rho v^2$
- Friction losses $\frac{1}{2}\rho v^2 \frac{fL}{D}$, where f is the friction loss coefficient, L is the length of the tube, and D is the inner diameter of the tube
- Geometry losses $\frac{1}{2}\rho v^2 k$, where k is the coefficient of losses due to bends, valves, etc.

Combining these terms, we see[1]:

$$P = \rho gh + \frac{1}{2}\rho v^2 + \frac{1}{2}\rho v^2 \frac{fL}{D} + \frac{1}{2}\rho v^2 k \tag{2.3.1}$$

$$= \rho gh + \frac{1}{2}\rho v^2 \left(1 + \frac{fL}{D} + k\right) \tag{2.3.2}$$

Markusic et al. [6] derive from the Lorentz (JxB) force the following relation for a DC conduction pump: $P = IB/s$. For the pump, B/s was measured to be 0.7 T/cm. For convenience, let $B_s = B/s$. Therefore,

$$P = \rho gh + \frac{1}{2}\rho v^2 + \frac{1}{2}\rho v^2 \frac{fL}{D} + \frac{1}{2}\rho v^2 k \tag{2.3.3}$$

$$= \rho gh + \frac{1}{2}\rho v^2 \left(1 + \frac{fL}{D} + k\right) \tag{2.3.4}$$

So the expression for current as a function of the parameters of the system, mainly the flow rate, is easily found from 2.3.4:

$$I = \frac{1}{B_s}\left[\rho gh + \frac{1}{2}\rho v^2 \left(1 + \frac{fL}{D} + k\right)\right] \tag{2.3.5}$$

[1]Some readers might note, correctly, the ρgh term would be dominant in most common conditions. However, it will later be shown that it will be advantageous to introduce conditions where the ρgh term is not in fact dominant.

It can be easily shown that, given the range of flow rates in the experiment, the flow in the lines will be laminar [2]; therefore, the friction factor f is given as $\frac{64}{Re} = \frac{64\mu}{\rho v D}$ by the Poiseuille equation. Starting from Eqn. (2.3.5), it is obtained:

$$\frac{1}{2}\rho v^2 \left(1 + \frac{fL}{D} + k\right) + (\rho g h - IB_s) = 0 \tag{2.3.6}$$

$$\frac{1}{2}\rho v^2 \left(1 + \frac{L}{D}\frac{64\mu}{\rho v D} + k\right) + (\rho g h - IB_s) = 0 \tag{2.3.7}$$

$$\frac{1}{2}\rho v^2 (1+k) + \frac{1}{2}\rho v^2 \frac{L}{D}\frac{64\mu}{\rho v D} + (\rho g h - IB_s) = 0 \tag{2.3.8}$$

$$\frac{1}{2}\rho (1+k) v^2 + \frac{32 L\mu}{D^2} v + (\rho g h - IB_s) = 0 \tag{2.3.9}$$

It is clear Eqn. (2.3.9) is quadratic in v. Solving, and disregarding the negative solution as non-physical, it is obtained:

$$v = \frac{\frac{-32\mu L}{D^2} + \sqrt{\left(\frac{32\mu L}{D^2}\right)^2 + 2\rho(1+k)(IB_s - \rho g h)}}{\rho(1+k)} \tag{2.3.10}$$

For a constant density flow, $\dot{m} = \rho v A$. The tube is of circular cross section, so $A = \pi(D/2)^2$ and $\dot{m} = \rho v \pi (D/2)^2 = (\rho v \pi D^2)/4$. Therefore, $v = 4\dot{m}/(\rho \pi D^2)$. Substituting, it is obtained:

$$\dot{m} = \frac{\pi}{4(1+k)}\left(-32\mu L + \sqrt{(32\mu L)^2 + 2\rho(1+k)(IB_s - \rho g h) D^4}\right) \tag{2.3.11}$$

Solve for I:

$$\left(\frac{4(1+k)\dot{m}}{\pi} + 32\mu L\right)^2 = (32\mu L)^2 + 2\rho(1+k)(IB_s - \rho g h) D^4 \tag{2.3.12}$$

$$\frac{\left(\frac{4(1+k)\dot{m}}{\pi} + 32\mu L\right)^2 - (32\mu L)^2}{2\rho(1+k)D^4} = IB_s - \rho g h \tag{2.3.13}$$

$$I = \frac{1}{B_s}\left[\frac{\left(\frac{4(1+k)\dot{m}}{\pi} + 32\mu L\right)^2 - (32\mu L)^2}{2\rho(1+k)D^4} + \rho g h\right] \tag{2.3.14}$$

As the EM pump is intended to be a drop-in replacement for the piston pump, it must

[2] At greatest, $\dot{m} = 100$ mg/s. Using the fact that flow velocity $v = \dot{m}/\rho A$, we see that Re= $\rho v D/\mu \approx 100$ for lithium in these conditions, thus placing the flow well in the laminar regime.

fit neatly into the existing apparatus. As such, the propellant lines must have a length L of 40 inches, height rise h of 25 inches. A pipe of inner diameter $D = 0.085$ inches is chosen. Density and viscosity of liquid lithium are functions of temperature, so they are taken to be the values near the melting point: $\rho = 512$ kg/m^3, and $\mu = 6 \times 10^{-4}$ Pa-s. The value of B_s inside the channel is 0.7 Tesla/cm. Minor losses are neglected here. ($k = 0$). Choosing $\dot{m} = 100$ mg/s to obtain the maximum current required and substituting, it is obtained that the necessary current $\boxed{I = 48.7 \text{ A}}$.

2.3.2 Power Supply Precision Requirement

In this section the required precision of the DC power supply (σ_I) will be calculated.

Recall Eqn. 2.3.11:

$$\dot{m} = \frac{\pi}{4(1+k)} \left(-32\mu L + \sqrt{(32\mu L)^2 + 2\rho(1+k)(IB_s - \rho g h)D^4} \right) \tag{2.3.15}$$

This expression clearly shows the functional relationship $\dot{m} = \dot{m}(k, \mu, L, \rho, I, B_s, g, h, D)$. Taylor [10] notes the uncertainty in a parameter such as $\dot{m}$ as a function of some variables x_i is given by:

$$\sigma_{\dot{m}} = \sqrt{\sum_i \left[\left(\frac{\partial \dot{m}}{\partial x_i} \right)^2 \sigma_{x_i}^2 \right]} \tag{2.3.16}$$

We seek a conservative estimate of σ_I; that is, we wish to err on the side of *over-predicting* σ_I. We therefore assume that *all* of the experimental uncertainty results from uncertainty in I. In other words, we assume σ_k, σ_μ, σ_L, σ_ρ, σ_{B_s}, σ_g, σ_h, and σ_D to be zero. Therefore, in this scenario,

$$\sigma_{\dot{m}} = \sqrt{\left(\frac{\partial \dot{m}}{\partial I} \right)^2 \sigma_I^2} \tag{2.3.17}$$

$$\sigma_{\dot{m}} = \left(\frac{\partial \dot{m}}{\partial I} \right) \sigma_I \tag{2.3.18}$$

Unfortunately, these computations (in particular, $\partial \dot{m}/\partial I$) become overly tedious to do analytically. Hence, they are done in the code in Appendix B. Results are shown in Figures 2.2 and 2.3.

2.3.3 Results and Implications for Power Supply Selection

Figure 2.2 shows the effect of tubing inner diameter on the current needed to achieve 100 mg/s flow rate (green) and the maximum allowed uncertainty in current σ_I needed to achieve ± 0.5 mg/s flow rate precision.

The trends makes intuitive sense. As tubing diameter decreases, friction losses increase. This means more current is required to generate enough pressure to push the lithium through the tube. Simultaneously, more "sloppiness" in current can be tolerated. As tubing diameter increases, the friction losses and flow velocity (and with this, the dynamic pressure $\rho v^2/2$) decrease, eventually becoming negligible with tubing of high inner diameter. Thus, the pressure required from the pump simply serves to generate enough head to lift the lithium into the thruster.

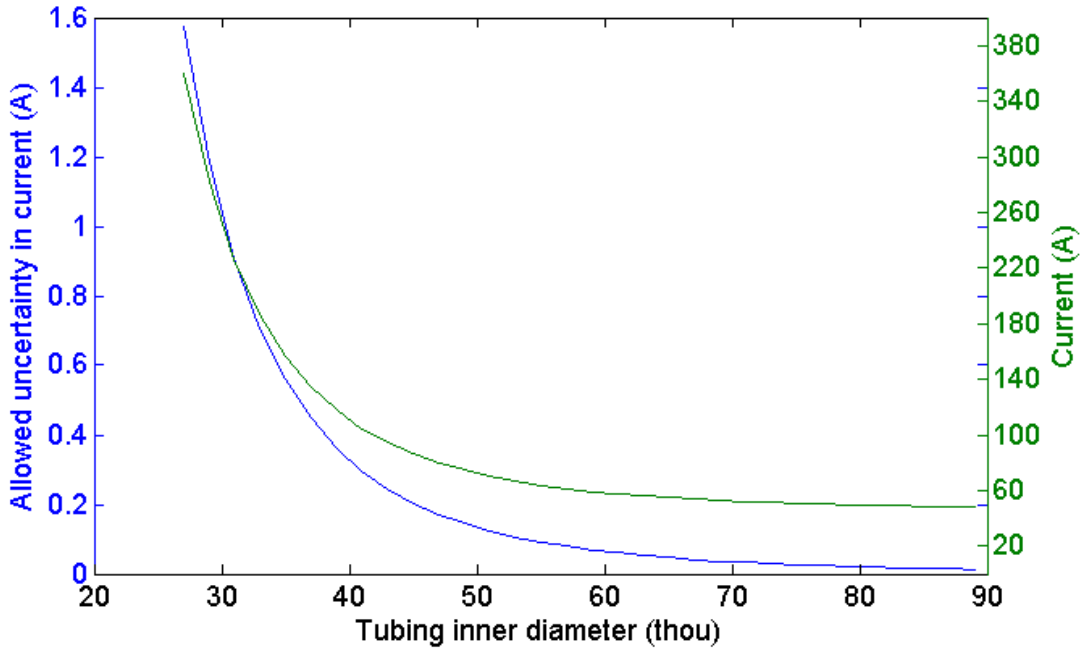

Figure 2.2: Current and maximum allowed uncertainty in current vs. tubing inner diameter. Values needed to achieve a flow rate of 100 ± 0.5 mg/s. The blue line is read from the left y-axis and the green line from the right y-axis.

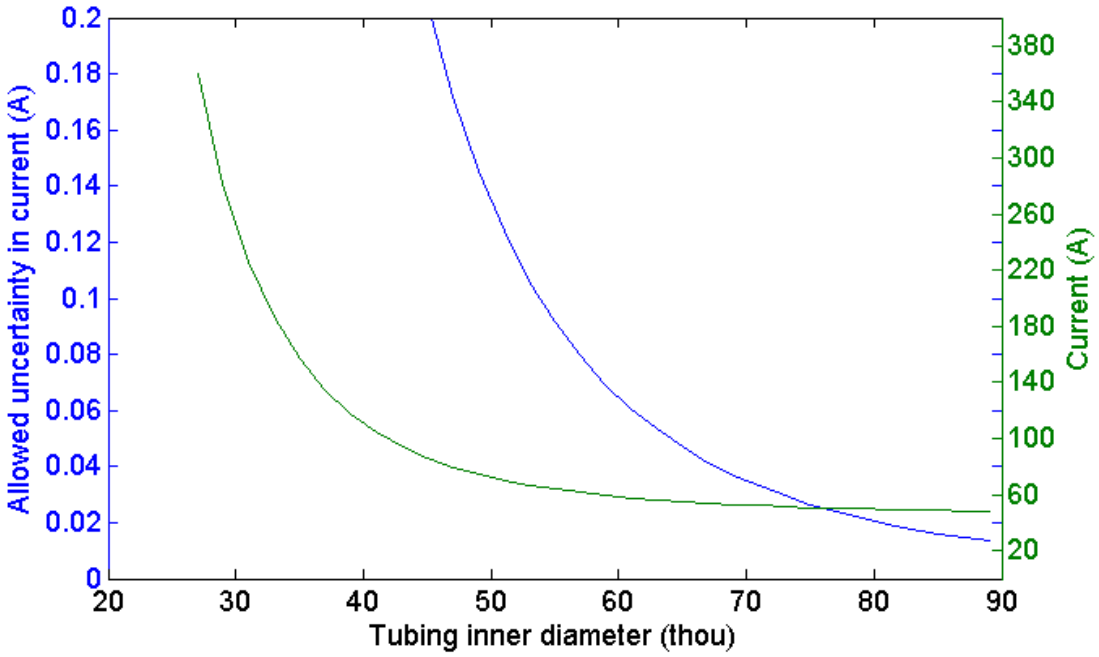

Figure 2.3: Zoomed-in version of Figure 2.2. The maximum allowed uncertainty in current at $D = 0.085$ in $= 16$ mA.

2.4 Power Supply Selection Process

It is clear that increasing pressure loss in the tubing allows us to increase σ_I, thus easing the requirements on the power supply. This is important, because a current-regulating DC power supply with both high range (over $\sim$10A) and high precision (less than $\sim \pm 100$ mA) is difficult to find for an affordable price. Much effort was spent on locating such a power supply.

The Acopian Y05LX7000 DC power supply was determined to meet the necessary criteria for tubing of inner diameter 0.040 inches. It has a maximum current of 70A and a programming accuracy of 350 mA. This satisfies the criteria, but with little margin.

In any case, given the assumptions going into this analysis, an experiment is necessary to decisively determine whether the EM pump can meet the requirements of the feed system. A prototype "shake-down" version of this experiment is presented in Chapter 3.

Chapter 3

Testing of EM Pump Feed System

3.1 Gallium vs. Lithium

Initial testing of the EM pump used gallium as a surrogate liquid metal for lithium. Initial testing is much easier to conduct with gallium because gallium is non-toxic and does not react with air or water, and thus does not need to be operated under vacuum. Another convenient aspect of gallium is its melting point of 30°C: just above room temperature.

Density, however, differs significantly: liquid lithium has a density of 0.512 g/cm^3, whereas liquid gallium has a density of 5.91 g/cm^3, roughly a tenfold difference. The viscosity of lithium is 6×10^{-4} Pa-s, whereas the viscosity of gallium is 12×10^{-4} Pa-s, a factor of two difference [1][2]. It should be noted that these values vary with temperature; but for our calculation purposes, they are taken to be the value close to the melting point, where the metals are most commonly operated.

The density difference between the metals becomes influential during pumping operations, since as we shall see the pressure P required is directly proportional to density ρ. The viscosity difference becomes important when frictional losses are high.

3.2 Experimental Setup

The parameters of the experiment were intended to be very roughly a gallium-scaled version of the lithium path. Thus the pressure head required was scaled by the density ratio (about 10), going from 25 inches for lithium to 2.5 inches for gallium. The tubing length was scaled by the viscosity ration, going from 40 inches for lithium to 20 inches

for gallium. This ensured the results would be somewhat comparable.

The apparatus consisted of a lowered resrvoir, the EM pump, and an elevated reservoir connected in series by SS316 tubing (ID 0.040 inch, OD 0.125 inch). The tubing was connected to the EM pump using a combination of Swagelok compression fittings and Swagelok VCR fittings. Both the lowered and the elevated reservoirs were SS316. To attach the tubing to the lowered reservoir, a hole was drilled, the tubing placed inside, and the seam was TIG welded.

The elevated beaker was placed on a Sartorius AY303 scale, with a readability of 5 mg. The scale was connected by a USB cable to a computer, where custom-written Python scripts logged scale readings and timestamps throughout the experiment.

The EM pump was connected to the Acopian Y05LX7000 power supply with 10 AWG wire, rated for 60 amps. The wire was attached to the tungsten electrodes with copper screw lugs and custom-milled clamping copper fittings.

A computer running a LabVIEW VI operated an NI USB-6211 data acqusition card. The 10V, 16-bit analog output of the USB-6211 was used to modulate the 10V control signal to the power supply.

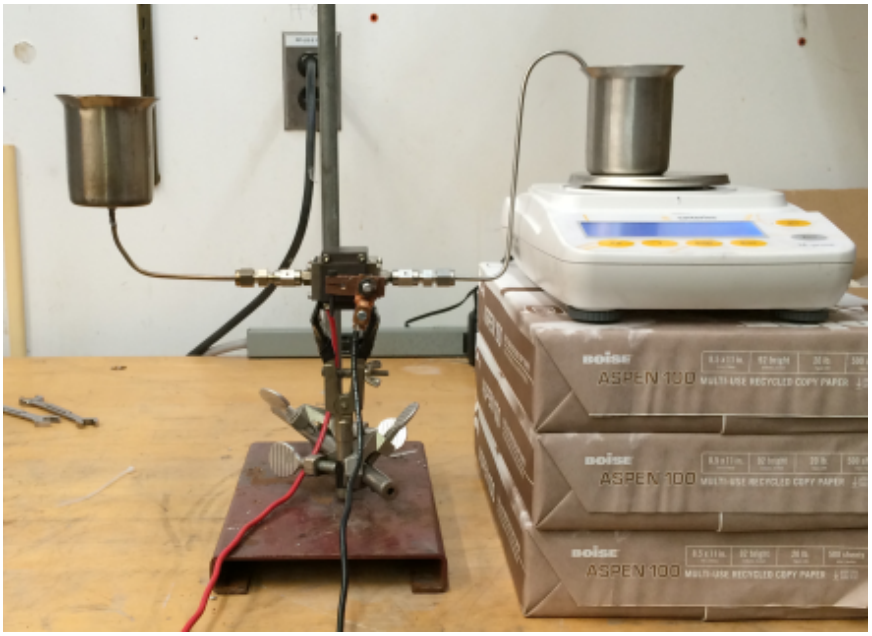

Figure 3.1: The testing apparatus. Gallium flows from left to right.

3.3 Procedure

A hot plate was used to melt gallium in a stainless steel beaker. The gallium was then poured into the lower reservoir. The entire apparatus was warmed with a heat gun, and then wrapped in ceramic insulation to prevent the gallium from freezing. The pump was primed by attaching a syringe with a rubber hose to the end of the tubing and applying suction, thus forcing gallium into the pump.

The LabVIEW VI was then started, which stepped progressively through higher currents until gallium exited the tube. The VI then stepped through the following currents, holding each for a minute: 27A, 27.5A, 28A, 28.5A, 29A. Data from the scale was logged by the Python script. Averaged flow rates were calculated by taking a best fit line through the mass/time data. The experiment was repeated three times.

3.4 Results and Conclusions

It is clear that the flow rate data collected lay well outside the range predicted by calculation. This finding is difficult to explain. Clearly the data is clustered around the correct values, but has a much higher variability than expected. Possible candidates for the discrepancy are:

- Gallium freezing in the lines. This was a problem early on, and was remedied by pre-warming the lines using the heat gun. If the experiment is to be repeated, the lines should be wrapped in active heating cables.

- Quantization error in the NI card. It is possible that the NI card introduces error into the control signal going into the power supply. This could be remedied by testing the outputs of the NI card and making sure they are properly calibrated before the test.

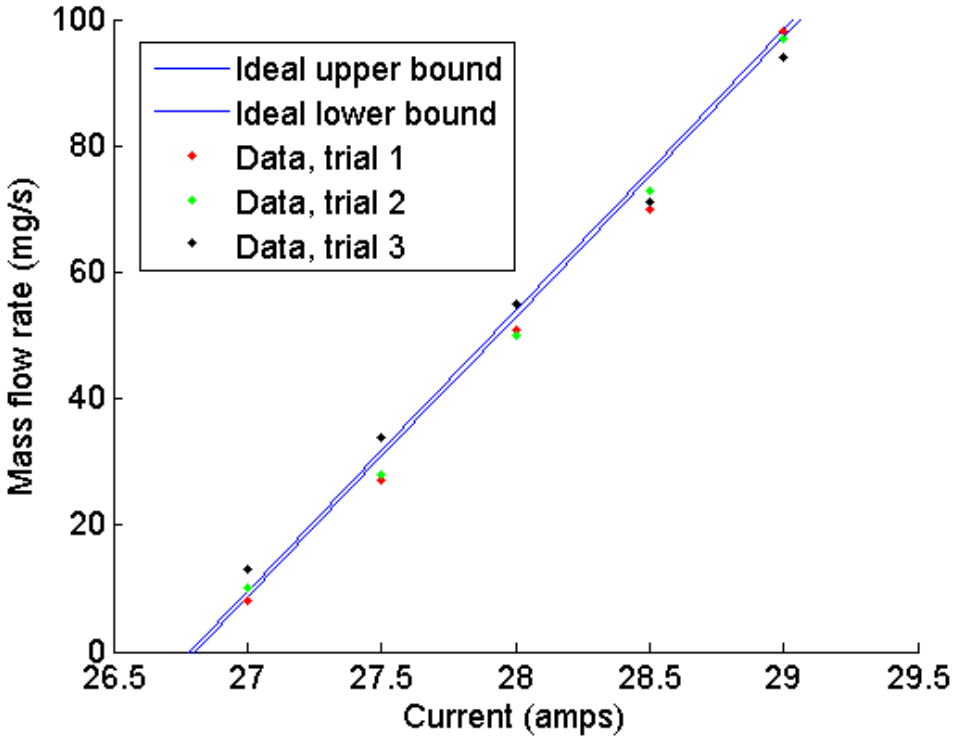

Figure 3.2: The blue lines represents the ideal flow rate from the equations. There are two lines because they represent the upper and lower bounds corresponding to ± 0.5 mg/s. The test data have error bars too small to see, because of the high precision of the scale (± 5 mg).

Chapter 4

Theory and Design of Laser Interferometer Flowmeter

4.1 Necessity of Mass Flowmeter

The necessity of a flowmeter is not immediately clear. By appropriate modulation of the current, the pressure generated by the pump can be set very precisely. One might suppose therefore that by appropriate modulation of the current, the mass flow into the thruster can be set precisely.

However, the analysis in Appendix A shows that the experimental uncertainty in viscosity (among other quantities) means that, by modulation of pressure alone, the mass flow cannot be set precisely enough for the goals of the apparatus. Therefore, a flowmeter is necessary to achieve anything near the desired flow rate precision.

4.2 Why Interferometer?

A flowmeter to be used in the LiLFA feed system has two important constraints. First, it must be very sensitive, able to measure flow rates as low as 10 mg/s. Second, it must be non-contact, due to the corrosive nature of liquid lithium. These two constraints eliminate most commercial flowmeter and level measurement instruments. To achieve measurements on the order of 10 mg/s, level measurements on the order of 1 μm are needed. There were two methods proposed to investigate: first, a laser interferometer; and second, a linearly actuated contact probe designed to measure the

height of the lithium surface. Given limited resources, it was decided to investigate the interferometer, because it has no moving parts to fail.

4.3 Laser Interferometers

Interferometers are a category of instruments that make measurements based on the interference of waves, typically light waves. Lasers are especially useful as a light source because all light in the beam has the same wavelength. A common configuration for interferometers is the Michelson-style configuration. In the Michelson interferometer, light, in our case, from a laser, is passed through a half-silvered mirror, whereupon it is split into two beams. One beam bounces off mirror 1 and the other bounces off mirror 2 (See Figure 4.1). The two beams then interfere at station E, where a screen may be located to display the interference pattern.

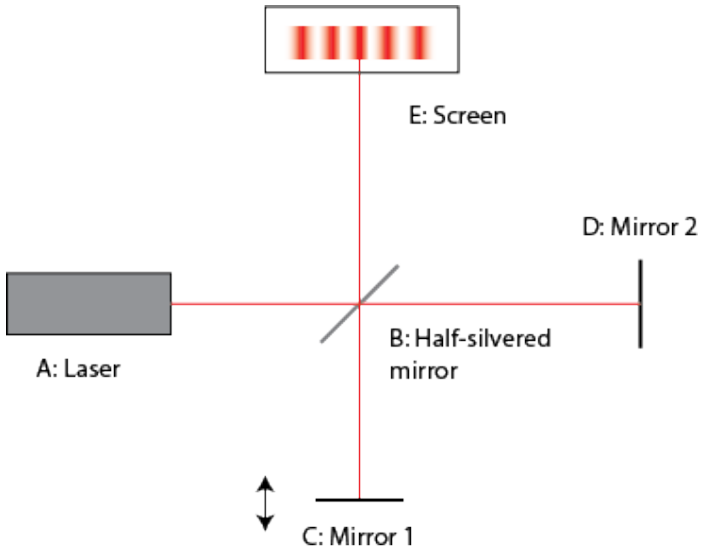

Figure 4.1: Schematic of a typical Michelson-style interferometer.

Figure 4.2 represents a level-measuring configuration of the interferometer. This strategy takes advantage of the fact that liquid lithium under vacuum forms a mirror surface. Therefore, the mirror at station C can be replaced by the lithium surface, and all the other optics aligned around it.

Then, as the lithium surface moves up or down, the laser beams fall out of phase, so the interference pattern changes. The fringe pattern would start to shift, sweeping from side to side as shown in Figure 4.3. If the fringes fall on a photodetector, then the photodetector could could fringes as they sweep across, and correlate it to a

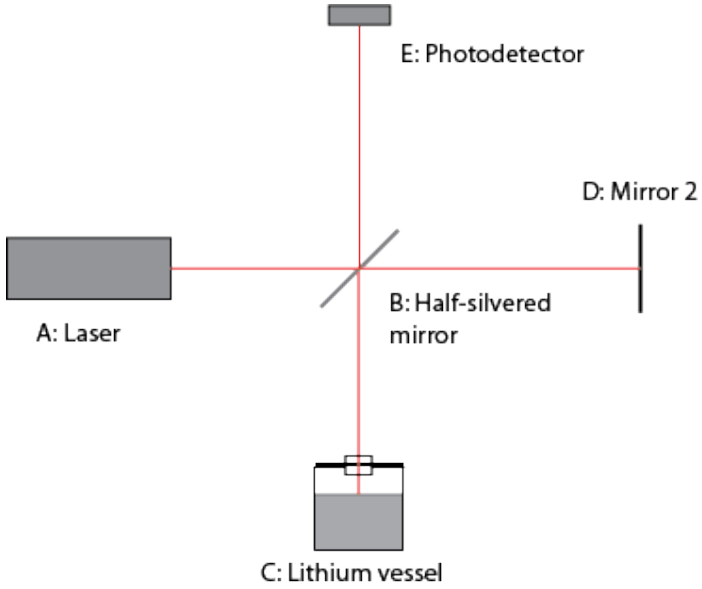

Figure 4.2: Schematic of the level-measuring interferometer configuration.

movement of the lithium surface. If n fringes are counted, then the distance d moved by the lithium surface is $n\lambda/2$, where λ is the wavelength of the light used.

Figure 4.3: Fringe sweeping.

Note that if the laser beams are aligned precisely, then one would expect to see circular fringes. Otherwise, parallel fringes are observed. However, precise alignment is not only difficult to achieve in practice, but also unnecessary. In fact, parallel fringes are required for the successful implementation of the fringe-sweeping strategy.

Chapter 5

Testing of Laser Interferometer Flowmeter Concept

5.1 Experimental Setup

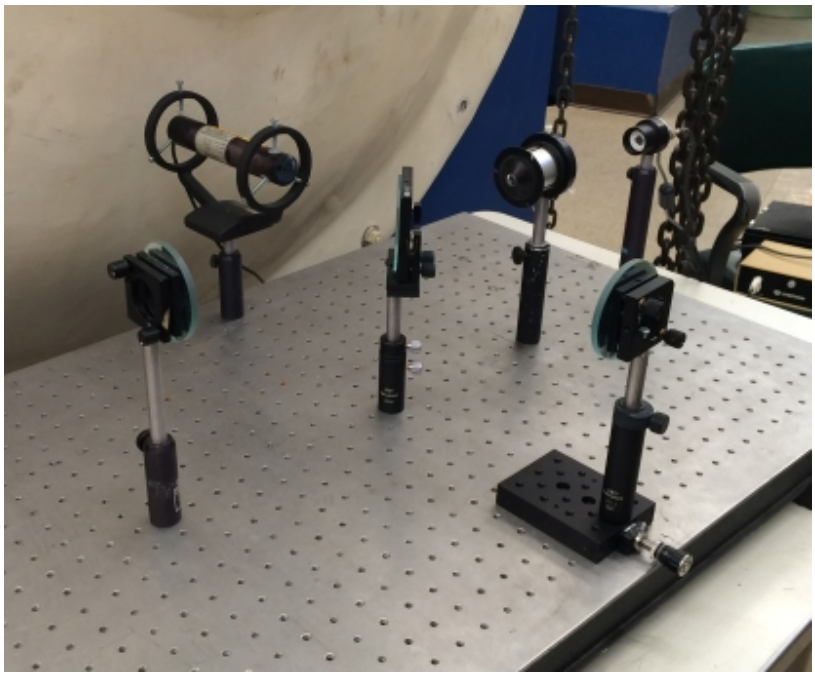

Figure 5.1: Interferometer setup.

A Michelson-style interferometer was set up to test the fringe-sweeping concept (see Figure 5.1). A 633 nm, 4 mW helium neon laser was used. The laser was passed

through a half-silvered mirror and bounced off two mirrors. One mirror was mounted on a smooth-action ball bearing translation stage with a differential adjuster, capable of displacements as small as 0.5 μm. The laser beams were aimed at a Thorlabs PDA155 photodetector, and the output was displayed on a Tektronix TDS3034B oscilloscope. The oscilloscope was connected via Ethernet to a computer, where waveform data was logged via a LabVIEW VI.

A microscope objective lens was placed between the half-silvered mirror and the photodetector in order to increase the size of the beam, thus increasing the size of the fringes. The lens was placed such that the width of a fringe was roughly the width of the sensitive region of the photodetector.

All components were mounted securely to an optics table. The table was placed on vibration-damping foam to isolate it from vibrations in the room.

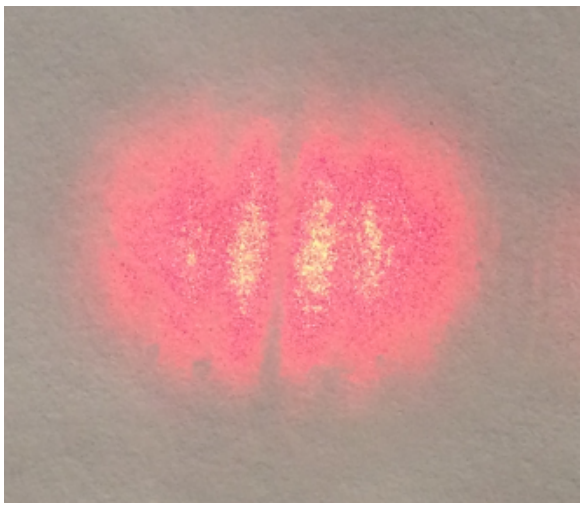

Figure 5.2: Example of interference pattern from the apparatus.

5.2 Results

The interferometer worked poorly as a displacement measuring instrument. The waveform signal was too noisy to observe any periodic variation in intensity that might be due to fringes sweeping over the photodetector. One noise filtering technique was applied. Harmonics of 60 Hz were discovered in the discrete Fourier transform (residue from AC line voltage), so a band-stop filter was applied to all frequencies within 10 Hz of the harmonics. A low-pass filter applied in conjunction also failed

to stop the noise. Perhaps with better signal processing, fringe sweeping could be observed.

Bibliography

[1] Marc J. Assael, Ivi J. Armyra, Juergen Brillo, Sergei V. Stankus, Jiangtao Wu, and William A. Wakeham. Reference data for the density and viscosity of liquid cadmium, cobalt, gallium, indium, mercury, silicon, thallium, and zinc. *Journal of Physical and Chemical Reference Data*, 41(3):–, 2012.

[2] Harry W. Davison. Compilation of thermophysical properties of liquid lithium. *NASA Technical Note D-4650*, July 1968.

[3] A. Forrester and F. Barcatta. Surface tension storage and feed systems for ion engines. *J. Spacecraft Rockets*, 3(7), March 1966.

[4] Andrea D. Kodys, Gregory Emsellem, Leonard D. Cassady, James E. Polk, and Edgar Y. Choueiri. Lithium mass flow control for high power lorentz force accelerators. *AIP Conference Proceedings*, 552(1), 2001.

[5] Daniel Lev and David Stein. *Lithium System Operation (EPPDyL Lab Manual)*. 2011.

[6] Thomas E. Markusic, Kurt A. Polzin, and Amado Dehoyos. Electromagnetic pumps for conductive-propellant feed systems. *29th International Electric Propulsion Conference*, 2005.

[7] Kurt A. Polzin and Thomas J. Godfroy. Flow components in a nak test loop designed to simulate conditions in a nuclear surface power reactor. *Space Technology and Applications International Forum (STAIF)*, 2008.

[8] Kurt A. Polzin and Thomas E. Markusic. Electromagnetic pumps for liquid metal-fed electric thrusters. *Journal of Propulsion and Power*, 23(6), 2007.

[9] John S. Snyder, Jeff Baldwin, Jason D. Frieman, Mitchel L.R. Walker, Nathan S. Hicks, Kurt A. Polzin, and James T. Singleton. Flow control and measurement

in electric propulsion systems: Towards an aiaa reference standard. *33rd International Electric Propulsion Conference*, 2013.

[10] John R. Taylor. *An Introduction to Error Analysis: The Study of Uncertainties in Physical Measurements*. University Science Books, 1997.

Appendix A

Uncertainty analysis

A.1 Contributors to Total Uncertainty

Start with Eqn. 2.3.11, derived in Chapter 2:

$$\dot{m} = \frac{\pi}{4(1+k)}\left(-32\mu L + \sqrt{(32\mu L)^2 + 2\rho(1+k)(IB_s - \rho g h)D^4}\right) \tag{A.1.1}$$

In general, L, ρ, g, h, and D can be measured to high precision. Moreover, these parameters are constant, and thus the influence of any uncertainty can be removed by a calibration; B_s falls into this category as well. This leaves k, μ, and I as variables with non-trivial uncertainties. Viscosity is the least certain parameter, so it tends to dominate the uncertainty in the result. In general, the uncertainty in the parameter $\dot{m}$ as a function of some variables x_i is given by Taylor [10]:

$$\sigma_{\dot{m}} = \sqrt{\sum_i \left[\left(\frac{\partial \dot{m}}{\partial x_i}\right)^2 \sigma_{x_i}^2\right]} \tag{A.1.2}$$

If we want to get a sense of the effect of the uncertainty in viscosity on the uncertainty in mass flow, we assume all other uncertainties are zero (i.e, $\sigma_{x_i} = 0$ for all x_i except viscosity). The contribution of the viscosity, then, becomes:

$$\sigma_{\dot{m}} > \sqrt{\left(\frac{\partial \dot{m}}{\partial \mu}\right)^2 \sigma_\mu^2} = \left|\frac{d\dot{m}}{d\mu}\sigma_\mu\right| \tag{A.1.3}$$

We find $\frac{d\dot{m}}{d\mu}$, and substitute to see:

$$\sigma_{\dot{m}} > \left| \frac{\pi}{4(1+k)} \left(-32L + \frac{1024L^2\mu}{\sqrt{(32\mu L)^2 + 2\rho(1+k)(IB_s - \rho gh)D^4}} \right) \right| \sigma_\mu \tag{A.1.4}$$

Clearly, since we have neglected all other uncertainties, this expression gives a *lower* bound on the uncertainty. It would be desirable to have this expression include $\dot{m}$. Transforming Eqn. (A.1.1), we see:

$$\sqrt{(32\mu L)^2 + 2\rho(1+k)(IB_s - \rho gh)D^4} = \frac{4(1+k)\dot{m}}{\pi} + 32\mu L \tag{A.1.5}$$

Substitute the square root term from Eqn. (A.1.5) into Eqn. (A.1.4) to get:

$$\sigma_{\dot{m}} > \left| \frac{\pi}{4(1+k)} \left(-32L + \frac{1024L^2\mu}{\frac{4(1+k)\dot{m}}{\pi} + 32\mu L} \right) \right| \sigma_\mu \tag{A.1.6}$$

$$> \left| \frac{\pi}{4(1+k)} 32L \left(-1 + \frac{32\mu L}{\frac{4(1+k)\dot{m}}{\pi} + 32\mu L} \right) \right| \sigma_\mu \tag{A.1.7}$$

$$> \left| \frac{\pi}{(1+k)} 8L \left(\frac{32\mu L - \frac{4(1+k)\dot{m}}{\pi} - 32\mu L}{\frac{4(1+k)\dot{m}}{\pi} + 32\mu L} \right) \right| \sigma_\mu \tag{A.1.8}$$

$$> \left| 8L \left(\frac{-4\dot{m}}{\frac{4(1+k)\dot{m}}{\pi} + 32\mu L} \right) \right| \sigma_\mu \tag{A.1.9}$$

$$> \left(\frac{8L\dot{m}}{\frac{(1+k)\dot{m}}{\pi} + 8\mu L} \right) \sigma_\mu \tag{A.1.10}$$

$$\Rightarrow \sigma_\mu < \left(\frac{\frac{(1+k)\dot{m}}{\pi} + 8\mu L}{8L\dot{m}} \right) \sigma_{\dot{m}} \tag{A.1.11}$$

Eqn. (A.1.11) allows us to find the maximum allowed uncertainty in viscosity needed to achieve an uncertainty of $\sigma_{\dot{m}}$ or less; that is, to achieve our desired mass flow rate with sufficient precision.[1] Substituting some typical values, $\dot{m} = 25$ mg/s, $k = 10$, $\mu = 6 \times 10^{-4}$ Pa-s, and our nominal desired mass flow precision, $\sigma_{\dot{m}} = 0.5$ mg/s, we see $\sigma_\mu = 2.00 \times 10^{-4}$ Pa-s.

By experimenting with Eqn. (A.1.11), we see that while L is a reasonable length (Say, $L <\approx 100$ in), the equation is largely insensitive to k, that is, until k approaches

[1] Note that, as we discussed, $\frac{d\dot{m}}{d\mu}\sigma_\mu$ significantly underestimates $\sigma_{\dot{m}}$ (see Eqn. (A.1.3)); this is because we have neglected all other uncertainties except that of μ.

unreasonable values: $k >\approx 10,000$. Moreover, the equation is insensitive to changes in L while k is a reasonably small value. Combining these two observations, we see that for reasonable values of k and L, the equation is insensitive to either value. This finding leads us to observe that, for reasonable values of k and L $\frac{(1+k)\dot{m}}{\pi} << 8\mu L$, so we can say:

$$\sigma_\mu <\approx \left(\frac{8L\mu}{8L\dot{m}}\right)\sigma_{\dot{m}} \tag{A.1.12}$$

$$\sigma_\mu <\approx \left(\frac{\mu}{\dot{m}}\right)\sigma_{\dot{m}} \tag{A.1.13}$$

$$\frac{\sigma_\mu}{\mu} <\approx \frac{\sigma_{\dot{m}}}{\dot{m}} \tag{A.1.14}$$

Naturally, the highest (worst-case) uncertainty in viscosity will come with the highest mass flow rate $\dot{m}$. So we take $\dot{m} = 25$ mg/s and $\sigma_{\dot{m}} = 0.5$ mg/s, and see that the fractional uncertainty in viscosity $\frac{\sigma_\mu}{\mu} = 0.02 = 2\%$.

Moreover, this equation tells us, given a certain σ_μ (from a reference, experiment, etc.), the minimum $\sigma_{\dot{m}}$ we can achieve.

A.2 Viscosity is the chief contributor to the total uncertainty

To summarize, if we make the liberal assumption that we have *perfect* knowledge of the quantities $k, \mu, L, \rho, I, B_s, g, h$, and D, and we desire to maintain a mass flow rate of $\dot{m} = 25$ mg/s to within an error of $\sigma_{\dot{m}} = 0.5$ mg/s, then it is necessary to know the viscosity μ to within an error of 2%. But there are four problems with this approach.

1. Viscosity varies significantly with temperature.

2. Viscosity cannot be measured to high precision, so reference texts often give a high uncertainty, typically on the order of several percent.

3. Reference texts vary widely on the value of viscosity itself. Values can differ by as much as 20% between references.

4. Because of our assumptions, this required precision of 2% significantly *under-predicts* the precision required. In reality, when we introduce the uncertainty of parameters such as I, we will require an uncertainty much less than 2% in order to achieve the flow rates we need.

For problem #1 (temporarily neglecting problems #2 and #3), we note that in order to know μ to within 2%, we need to know temperature to within approximately 10°C, necessitating the introduction of instrumentation to determine the lithium temperature. However, problems #2 and #3 are more severe.

A.3 Resolution

Note that this issue resulting from uncertainty in viscosity is not unique to lithium; it is relevant for any system that attempts to control downsteam mass flow precisely by control of upstream pressure alone. The solution, in many cases, is simple—install a flowmeter downstream and use feedback control. Of course, in the case of LiLFA, conventional flowmeters are not practical, for reasons given in Section 2.1: the corrosiveness of lithium and the high precision of mass flow required.

Appendix B

MATLAB: uncertainty.m

```
% assume minor loss term k = 0

% head required of pump, in
head = 25;
head = head*0.0254; % m
% length tubing needed, in
l_tube = 40;
l_tube = l_tube*0.0254; % m
% desired mass flow, mg/s
mdot_desired = 100;
mdot_desired = mdot_desired*1e-6; % kg/s
% density, kg/m3
density = 512;
% viscosity, Pa-s
viscosity = 6e-4;
% magnetic field strength, T/m
Bs_val = 70;

% initiate symbolic variables
% v=flow velocity, c=current, rho=density, Bs=magnetic field
% g=gravity accel, h=head, L=length tubing, D=diameter tubing,
% mu=viscosity
syms v c rho Bs g h L D mu;
% eqn 2.1.2 from thesis (UPDATE THIS)
```

```
eqn = 0.5*rho*v^2*(1+64*mu*L/rho/v/D^2) + rho*g*h - c*Bs;
% set eqn = 0, solve for flow velocity v
soln = solve(eqn,v);
% take only the positive solution
v = soln(1);
% convert flow velocity to mass flow rate
mdot = v*rho*(pi*(D/2)^2);

% initialize another mdot symbolic for dummy purposes
syms mdot2;
% range of reasonable values of tubing diameter
D_vals = 0.027:0.002:0.090;
% initialize counter
i = 1;

% loop through tubing diameters
for D_iter = 0.027:0.002:0.090
    % partial derivative of mdot wrt current
    % differentiate mdot wrt c, replace irrelevant terms with
    % relations involving mdot; "calibration"
    dmdot_dc = simplify(subs(diff(mdot,c),...
        (- g*h*D^4*rho^2 + Bs*c*D^4*rho + 512*L^2*mu^2),...
        0.5*(mdot2*4/pi+32*mu*L)^2));
    % sub in values into derivative of mdot wrt c
    dmdot_dc_val = subs(dmdot_dc, ...
        [Bs, D, rho, L, mu, mdot2],...
        [Bs_val, D_iter*0.0254, density, l_tube, ...
        viscosity, mdot_desired]);
    % uncertainty in mdot
    mdot_sig = 0.5e-6;
    % evaluate according to eqn 2.4.12 (UPDATE)
    % uncertainty in current
    c_sig(i) = mdot_sig/dmdot_dc_val;

    % initialize another mdot symbolic for dummy purposes
    syms mdot3;
```

```
    dummy = mdot3 - mdot;
    % set dummy = 0, solve for current
    Icur = solve(dummy, c);
    % value of current
    c_val(i) = subs(Icur, [g h D rho mdot3 L mu Bs],...
        [9.8 head D_iter*0.0254 density mdot_desired ...
        l_tube viscosity Bs_val]);

     i = i + 1;
end

figure
% set(gca,'FontSize',14)
% set(findall(gcf,'type','text'),'FontSize',14)
[ax, p1, p2] = ...
    plotyy(1000*D_vals, c_sig, 1000*D_vals, c_val)
ylabel(ax(1), 'Allowed uncertainty in current (amps)', ...
    'FontSize',14)
ylabel(ax(2), 'Current (amps)', 'FontSize',14)
xlabel('Tubing inner diameter (thou)', 'FontSize',14)
set(ax(1),'YTick',0:0.2:2, 'FontSize',14)
set(ax(2),'YTick',20:20:200, 'FontSize',14)
```